

Bridging the gap between conventional and video-speed scanning probe microscopes

A.J. Fleming^{a,*}, B.J. Kenton^b, K.K. Leang^b

^a School of Electrical Engineering and Computer Science, University of Newcastle, Callaghan, NSW 2308, Australia

^b Department of Mechanical Engineering, University of Nevada—Reno, Reno, NV 89557-0312, USA

ARTICLE INFO

Article history:

Received 15 February 2010

Received in revised form

18 April 2010

Accepted 27 April 2010

Keywords:

Tip scanning instrument design and characterization

Scanning tunneling microscopy (STM)

Atomic force microscopy (AFM)

ABSTRACT

A major disadvantage of scanning probe microscopy is the slow speed of image acquisition, typically less than one image per minute. This paper describes three techniques that can be used to increase the speed of a conventional scanning probe microscope by greater than one hundred times. This is achieved by the combination of high-speed vertical positioning, sinusoidal scanning, and high-speed image acquisition. These techniques are simple, low-cost, and can be applied to many conventional microscopes without significant modification. Experimental results demonstrate an increased scan rate from 1 to 200 Hz. This reduces the acquisition time for a 200 × 200 resolution image from 3 min to 1 s.

© 2010 Elsevier B.V. All rights reserved.

1. Introduction

In addition to topographic imaging, the scanning probe microscope (SPM) has provided a window into the operation of physical interactions at the micro- and nanoscale. These interactions include electrical and mechanical forces, chemical bonding, and biological processes [1–5]. Due to the unique imaging capabilities and wide range of use, there has been a dramatic increase in the number of imaging modes and sensors since the invention of the atomic force microscope (AFM) in 1986 [6]. However, in this same period, the speed of standard scanning probe microscopes has not kept pace with other aspects of the technology. For example, with a typical scan-rate of 1 Hz, a single image may take minutes to acquire. In many applications, this lengthy imaging time is simply an inconvenience; however, in other applications, the low speed becomes a critical limitation. Examples where speed is a primary concern include: large-range surface inspection [7,8], nanofabrication [9–12], and imaging of fast biological and physical processes [13–16].

There are four major factors that limit the speed of scanning probe microscopes. These are: the resonance frequency or bandwidth of the probe; the resonance frequency or bandwidth of the scanner; the bandwidth of the acquisition system; and finally, the closed-loop bandwidth of the vertical feedback

controller. Detailed reviews of these limitations can be found in Refs. [17–21].

In recent years, a considerable improvement in the speed of scanning probe microscopes has been achieved with the introduction of advanced control techniques. These include actuator linearization [22–24], feedforward control [25], input shaping [26,27], and improved feedback control [23,28–30]. Although such techniques have been demonstrated to improve speed, widespread application has been limited by the degree of implementation complexity. Significant modifications to the hardware or operating logic of the microscope are typically required. Such changes may be difficult or impossible to implement in many commercial SPMs.

To service the growing demand for high-speed microscopy, dedicated video-speed microscopes have been developed [14,21,28,31–34]. Commercial implementations are also available from Infintesima, UK, and Olympus, Japan. Video-speed microscopes are highly optimized for contact-mode or tapping-mode imaging and are capable of recording more than 30 images per second. However, a consequence of the highly optimized design is that video-speed AFMs may not be suitable for general purpose applications that can require: large scan areas, large sample sizes or the use of a wide variety of imaging modes and probe types.

The most recent generation of general purpose AFMs have also responded to the demand for higher speed. A number of manufacturers are now offering microscopes capable of operating in constant-force mode with line-rates on the order of 50 Hz or greater.

* Corresponding author. Tel.: +61 2 4921 6493; fax: +61 2 4921 6993.

E-mail addresses: andrew.fleming@newcastle.edu.au (A.J. Fleming), kam@unr.edu (K.K. Leang).

In order to close the gap between standard SPMs and dedicated video-speed microscopes, this paper demonstrates three simple techniques that can reduce the image acquisition time of a 200×200 resolution image from 3 min to 1 s. The proposed techniques are straight-forward to implement and are easily retrofitting to standard commercial SPMs.

The first difficulty encountered when increasing the scan-rate is oscillation of the lateral scanner. In this work, sinusoidal trajectories are used to eliminate harmonic excitation of the scanner resonance modes. This approach was first used for AFM by Humphris, Miles and Hobbs in 2005 [32]. The sample was mounted on a tuning fork oscillating at its resonance frequency. Later, a more practical configuration was demonstrated where the probe is oscillated rather than the sample [34].

Sinusoidal scanning has also been applied to standard microscopes with piezoelectric tube scanners. The technique of spiral scanning was first discussed in 2003 [35] then applied to AFM imaging in 2008 [36]. Spiral scanning involves the application of sine- and cosine-waves to the x - and y -axis of a piezoelectric tube scanner. The signal amplitude is ramped upwards so the probe ‘spirals’ outward from the center. The main drawbacks reported in [36] were the non-uniform spatial sampling, the need for interpolation onto a normal grid, and the non-constant velocity. In addition, the driving signals are ramped-sinusoids, not perfect sinusoids, so they do not have an impulsive spectrum and can excite mechanical resonance frequencies, albeit to a much lesser extent than a standard triangular scan pattern. Further details on spiral scanning and some other similar patterns can be found in the patent filed in 2007 [37]. Experimental constant-height images can also be found in Ref. [38].

In this work, the fast scan-axis of a piezoelectric tube scanner is driven with a pure sinusoid. This simple approach is similar to the tuning-fork method [32,34] except that the tube is driven at an arbitrary frequency. Compared to spiral scanning, the applied signal is a single tone and the image is at least uniformly sampled in one direction. This technique was recently used for high-speed nanofabrication [39]. In Section 3, sinusoidal scanning is demonstrated to increase the maximum scan-rate of a piezoelectric tube scanner from approximately 1 to 200 Hz.

After the scanning performance of an SPM is improved, the major speed limitation becomes the vertical feedback bandwidth. This control loop regulates the tip-sample interaction in application modes such as constant-current STM and constant-force AFM. An introduction and review of this topic can be found in Refs. [17–21,40]. In Ref. [17], the maximum vertical feedback bandwidth with an integral controller is shown to be equal to the lowest scanner resonance frequency divided by the peak amplitude, that is

$$\text{max. bandwidth} < \frac{\omega_1}{P}, \quad (1)$$

where ω_1 is the first resonance frequency and P is the magnitude at the resonance frequency divided by the DC-Gain. This definition of P is convenient as it can be measured directly from a frequency response plot. On the decibel scale, P is simply the height of the resonance peak above the DC-Gain; however, if P is measured in this way, it must be converted from dB into a linear quantity. For example, the scanner used in this work has a resonance frequency of 680 Hz and a 15-dB difference between the DC-Gain and resonance peak, which equates to $P=5.6$. This implies a bandwidth limit of approximately 120 Hz, which is sufficient for a scan-rate of around 1 Hz and an image acquisition period of more than 3 min with a resolution of 200×200 .

To image a sample with relatively sharp features, the vertical feedback bandwidth must be approximately one-hundred times the scan-rate. This rough approximation assumes a triangular scanning pattern, five features per line, and a spatial bandwidth of ten times

the period of each feature. In order to increase the imaging rate to one frame-per-second at 200×200 resolution, the vertical feedback bandwidth needs to be increased by more than two orders of magnitude to greater than 20 kHz. Unfortunately this is impossible to achieve with a piezoelectric tube scanner. To overcome this limitation, a high-speed vertical positioner is required.

It is also possible to avoid the need for a feedback loop by operating in constant-height mode. However, constant-force techniques are generally preferred and specialized cantilevers may be required to avoid sample damage [32].

To obtain a wide vertical feedback bandwidth, video-speed AFMs contain specialized high-speed positioners. Mechanical designs have included shear-mode actuators [33], balanced scanners [31], and flexure-based designs [15]. Another method for increasing the resonance frequency is to actuate the probes directly, this has been demonstrated with piezoelectric probes [41], magnetic probes [42], and electrostatic probes [43]. Although these specialized techniques can achieve high bandwidth, they may not be practical for general purpose applications.

In recent years, considerable research has also proceeded to increase the vertical feedback bandwidth of standard microscopes. Although model-based control offers a significant improvement [13], the most dramatic increases have resulted from the addition of an auxiliary high-speed vertical actuator [17,20,44,45]. The foremost disadvantages of these ‘dual-stage’ techniques are the increased complexity, and low range of the high-speed actuator.

Over the period where model-based and dual-stage control was under development, commercial AFM manufacturers began to eliminate lateral scanner dynamics from the vertical feedback loop. A number of current models now use separate lateral and vertical positioning systems. Since the vertical positioner need only drive the small cantilever mass, the resonance frequency can be extremely high [46].

In this work, a high-speed vertical positioner is described that can be easily retrofitted to many existing microscopes. Since it is difficult to modify or interfere with the cantilever holder and optical system, the positioner in Section 4 is designed to drive the sample mass. A balanced mechanical design [31] is used together with a new circular flexure to achieve a range of $2.3 \mu\text{m}$ and a resonance frequency of 103 kHz. With a simple analog integral controller, the closed-loop bandwidth is increased from 83 Hz to 67 kHz, which is easily sufficient to achieve one frame-per-second at 200×200 resolution.

The final improvement, described in Section 5, is a low-cost hardware and software solution for data acquisition and presentation. This package allows video-speed imaging and includes all of the functionality required to incorporate the above techniques into a standard SPM.

This paper proceeds with a description of the experimental apparatus in the following section. Sinusoidal scanning is then discussed in Section 3 followed by vertical feedback in Section 4, and data acquisition in Section 5. Imaging experiments are presented in Section 6 that demonstrate the efficacy of these techniques. Conclusions are drawn in Section 7.

2. Experimental setup

In this work, an NT-MDT Ntegra scanning probe microscope, pictured in Fig. 1, is used to demonstrate the proposed techniques. The scanner is an NT-MDT Z50309cl piezoelectric tube scanner with $100\text{-}\mu\text{m}$ lateral range and $10\text{-}\mu\text{m}$ vertical range. The scanner comprises two piezoelectric tubes joined at the base. One tube is used for lateral positioning, and the other for vertical positioning. This configuration results in a lateral resonance frequency of 680 Hz, which is typical for a tube scanner with $100\text{-}\mu\text{m}$ range. Frequency response measurements can be found in Ref. [47].

A signal access module allows direct access to the cantilever deflection, scanner electrode voltages, and reference trajectory.

The cantilever is a TR800PSA Olympus Biolever with a resonance frequency of 73 kHz and a stiffness of 0.57 N/m.

3. Lateral scanning trajectories

It is well known that triangular scanning trajectories result in oscillation at scan-rates above approximately 1% of the resonance frequency. This is demonstrated in Fig. 2(a). With a scan-rate of 10 Hz, the lateral vibration becomes intolerable at 2% of the scan range. Above this frequency, triangular scanning is not feasible.

As discussed in the introduction, the maximum scan-rate can be improved by the application of feedback, feedforward and input shaping control. However, the implementation of such techniques is complicated as many commercial microscopes either do not have position sensors or access to the signals is not provided. This renders the majority of advanced control

techniques either difficult or impossible to implement without significant modification.

If position sensors are not available or if additional complexity is undesirable, the only available option is modification of the driving signal applied to the scanner. A range of published driving signals were compared in Ref. [27]. Although a subset of these techniques were able to provide regions of constant probe velocity, some knowledge of the scanner dynamics was required.

A simpler alternative to triangular scanning is sinusoidal scanning. Unlike triangular or semi-triangular trajectories, sine waves contain no harmonics that can excite mechanical resonances. This allows an order-of-magnitude increase in scan-rate. In addition, any known scanner dynamics can be inverted with a simple change of magnitude and phase. The disadvantage of sinusoidal scanning is the non-constant probe velocity which is unsuitable for some imaging techniques such as lateral-force mode.

Due to the high achievable scan rate, sinusoidal scanning is used in some video-speed microscopes by exciting a tuning fork at its resonance frequency [32]. If constant-probe velocity is a necessity, the optimal signal proposed in [27] is recommended. Other recommended scan trajectories include the shaped signal in [48] and the semi-parabolic waveform in [33].

The benefits of sinusoidal scanning are clearly evident in Fig. 2(b). Negligible vibration is observed up to approximately 200 Hz. At this frequency, the third harmonic (due to piezoelectric non-linearity) begins to excite the mechanical resonance. Sinusoidal scanning can be used up to, and indeed well above the scanner resonance frequency; however, best results are obtained when the third harmonic does not lie near a mechanical resonance. The upper speed limit of sinusoidal scanning occurs when the vertical modes of the scanner become excited, this causes significant image distortion.

4. Vertical feedback enhancement

4.1. Vertical feedback limitations

The vertical feedback system for an atomic force microscope operating in constant-force contact-mode is illustrated in Fig. 3(a). The piezoelectric tube scanner moves the probe in a



Fig. 1. The NT-MDT Ntegra scanning probe microscope arranged in a scan-by-probe configuration. The scan head is mounted above a stationary sample platform.

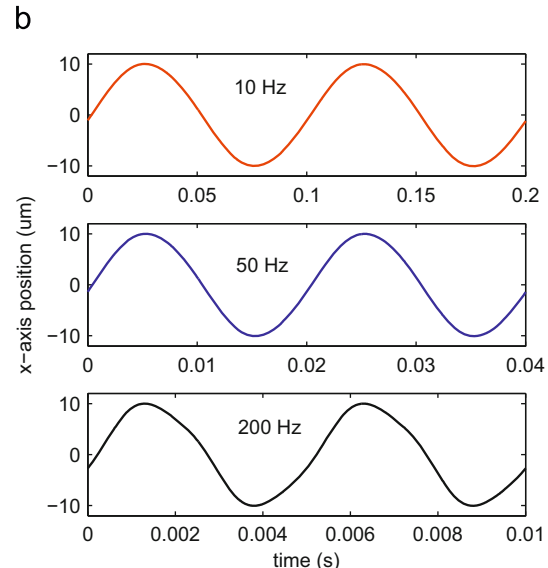
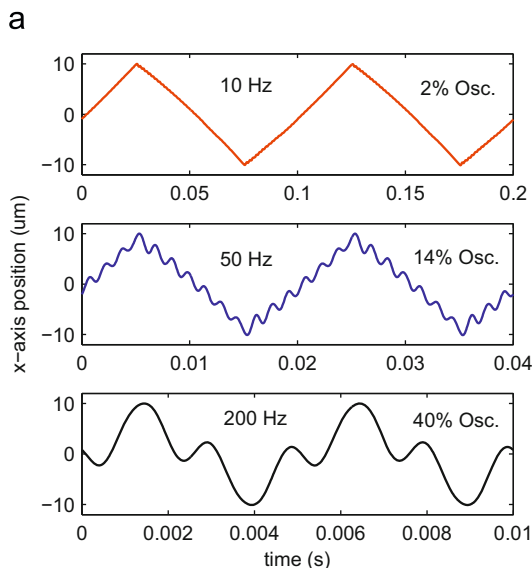


Fig. 2. The resulting scanner displacement with triangular and sinusoidal lateral scanning trajectories. The peak-to-peak oscillation in percent of the total scan range is also shown in (a). (a) Triangular scanning and (b) sinusoidal scanning.

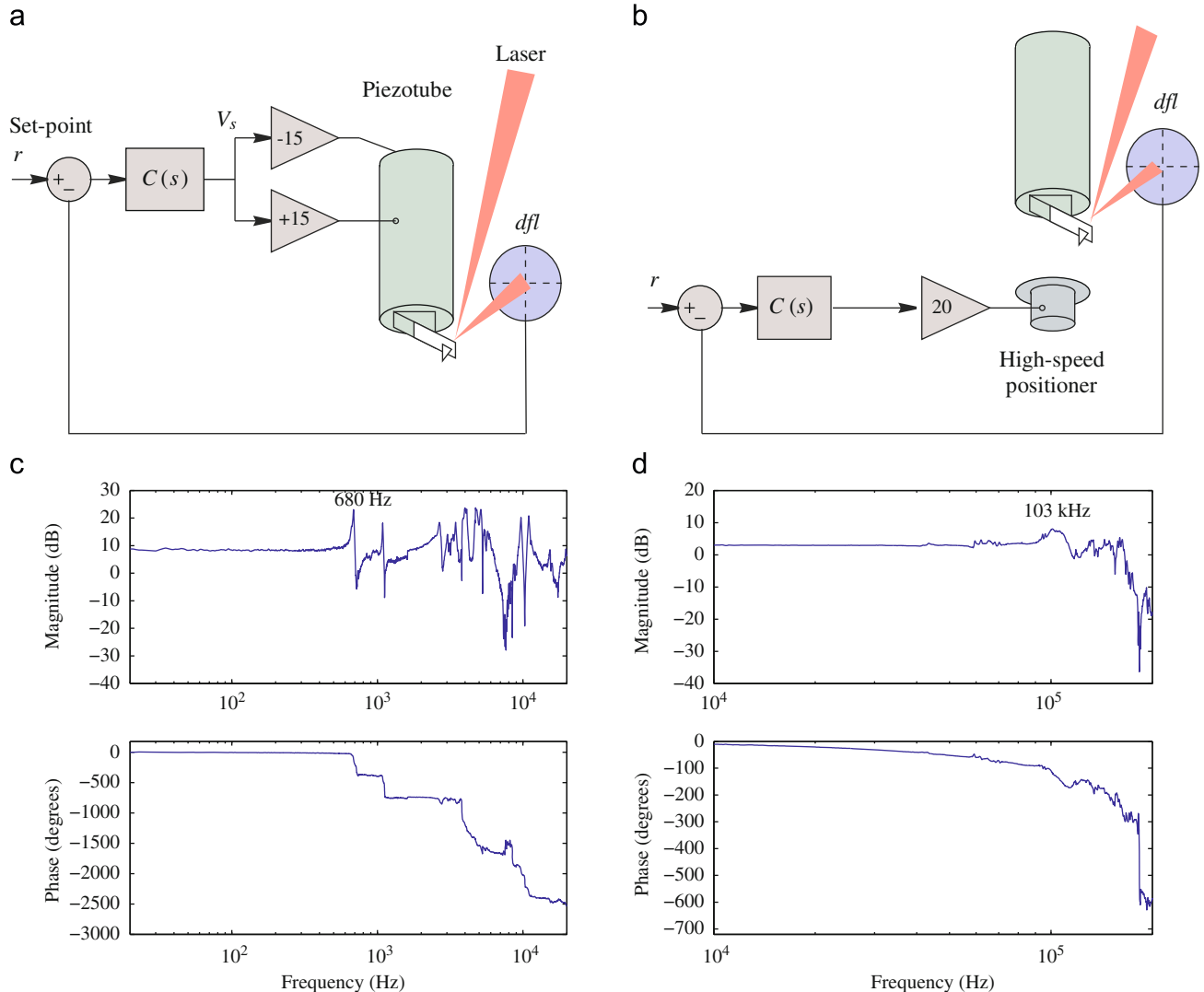


Fig. 3. The schematic diagram and frequency response of a standard and high-speed vertical feedback system. The frequency responses were measured from the applied voltage V_s to the cantilever deflection dfl . From (d), the resonance frequency of the high-speed stage is 103 kHz, this is 150 times faster than the piezoelectric tube. (a) Standard vertical feedback control loop, (b) high-speed vertical feedback control loop, (c) standard vertical frequency response $G_{dV_s}(j\omega)$, and (d) high-speed vertical frequency response $G_{dV_h}(j\omega)$.

vertical direction to regulate the cantilever deflection dfl to a set-point r . Although the diagram in Fig. 3(a) represents an AFM operating in constant-force contact-mode, this schematic is similar to all forms of SPM where the tip-sample interaction is controlled. Different operating modes use different feedback variables. For example, in constant-force contact-mode AFM, the feedback variable is cantilever deflection. In constant-current STM, the feedback variable is tunneling current. Other feedback variables include the cantilever oscillation magnitude in tapping-mode AFM and the fiber oscillation magnitude in scanning near-field optical microscopy. All of these modes share the same feedback system but with different feedback variables or methods of detection.

The simplest and most commonly used vertical feedback controller $C(s)$ is an integral controller, i.e.,

$$C(s) = \frac{\alpha}{s}. \quad (2)$$

Integral controllers are popular because they are simple to implement, provide good regulation of tip-sample interaction at low frequencies, and are easily adjustable. Ease of tuning is a

necessity as the feedback system must accommodate many different imaging modes and cope with a wide range of probes and samples. However, in spite of the additional complexity, some high performance microscopes have used model-based controllers; examples include [13,21,44].

The frequency response of the standard vertical feedback system is plotted in Fig. 3(c). This response is measured from the control voltage V_s to the deflection dfl . The system under consideration includes the amplifier dynamics, the scanner and cantilever mechanics, and the tip-sample interaction. The composite system is denoted G_{dV_s} , where

$$G_{dV_s}(s) = \frac{dfl(s)}{V_s(s)}. \quad (3)$$

The frequency response of $G_{dV_s}(s)$ is essentially flat from DC to 680 Hz where the first resonance frequency of the scanner occurs. This resonance is due to the first lateral bending mode of the tube which is coupled into the vertical response [49].

As discussed in the introduction, the resonance at 680 Hz limits the vertical feedback bandwidth to only 120 Hz. In practice, however, the bandwidth is even lower as the controller gain must

be reduced in order to provide sufficient stability margins. The expression for maximum bandwidth in Eq. (1) can be modified to include a term for gain-margin [17],

$$\text{max. bandwidth} = \frac{\omega_1}{P} \times \frac{1}{\text{gain-margin}}. \quad (4)$$

The maximum controller gain α can also be determined [17],

$$\alpha_{\text{max}} < \frac{\omega_1}{PG_{dv_s}(0)} \times \frac{1}{\text{gain-margin}}, \quad (5)$$

where $G_{dv_s}(0)$ is the open-loop DC-gain, and gain-margin is the additional gain the control loop will tolerate before instability occurs. Gain-margin is the foremost limitation when dealing with integral control of resonant systems.

With a reasonable gain-margin of 5 dB, the maximum controller gain is $\alpha = 190$ which results in a predicted maximum vertical feedback bandwidth of 68 Hz [17]. In experiments, the measured closed-loop bandwidth was 83 Hz [17]. This is only sufficient for line-rates of approximately 1 Hz or less. The response of the controller with a 10 Hz line-rate is shown in Fig. 4. The inadequate vertical feedback bandwidth ‘smudges’ the feature edges. In the following section, the vertical feedback bandwidth is improved by replacing the standard vertical positioner with a high-speed piezoelectric stack actuator.

4.2. High-speed vertical positioning

The foremost bandwidth limitation of the vertical feedback system is the low resonance frequency of the piezoelectric tube scanner. To increase the imaging speed to one frame-per-second, the closed-loop bandwidth requires an increase of more than two orders of magnitude. As discussed in Section 1, this can be achieved by replacing the vertical positioning function of the piezoelectric tube with a high-speed piezoelectric stack actuator. Such an arrangement is illustrated in Fig. 3(b). Here the piezoelectric tube is used only for lateral scanning while the high-speed

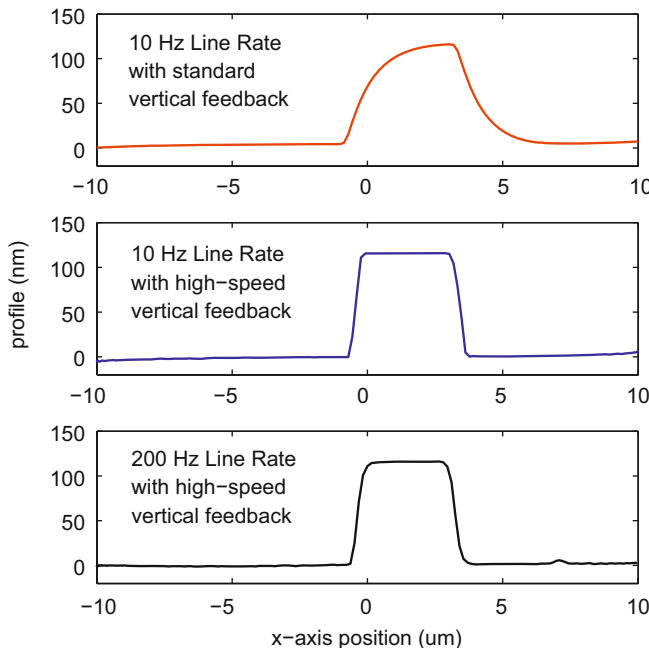


Fig. 4. A single image line of a $20 \times 20 \mu\text{m}$ constant-force scan. With the standard vertical feedback controller (83 Hz bandwidth) shown at top, the controller is too slow to accurately track sharp sample features. With the use of high-speed vertical feedback (67 kHz bandwidth), the sample features are accurately captured at both 10 and 200 Hz line-rate.

actuator is used for vertical feedback. This configuration is similar to dual-stage actuation [17,20,44,45] except that the high-speed positioner in Fig. 3(b) is designed for full-range, which simplifies the control and microscope integration substantially. In addition, since the high-speed actuator drives the sample rather than the probe [46], no modifications to the cantilever holder or optics are necessary.

Due to their low mass and high stiffness, small piezoelectric stack actuators can provide extremely high resonance frequencies. For example, a 2-mm thick plate-stack actuator with a cross section of $5 \times 5 \text{ mm}$ (Noliac CMAP07) has a free stroke of $3.1 \mu\text{m}$ and an unloaded free resonance frequency of greater than 500 kHz. The nominal capacitance of this actuator is 100 nF which requires a low output-impedance amplifier to achieve the full bandwidth. The same plate-stack actuator is available with ceramic end caps for electrical isolation (Noliac SCMAP07), this offers $2.9 \mu\text{m}$ of travel and an unloaded free resonance frequency of greater than 250 kHz (total actuator length is 4 mm). Another comparable actuator is the PICMA chip actuators available from Physik Instrumente. In practice, the travel range and the resonance frequency is reduced by the boundary conditions, additional sample mass, and end-caps.

Several possibilities for integrating a plate- or ring-stack actuator into an SPM are illustrated in Fig. 5. The simplest arrangement is the fixed-free situation illustrated in Fig. 5(a). Here the base of the actuator is bonded to a rigid platform and the sample mass m is attached to the free end. Although simple, this configuration is not ideal for a number of reasons. First, if the total length of the actuator including the sample mass is relatively long compared to the transverse dimensions, the first resonance will be a bending mode. This causes the sample to displace side-to-side as well as up and down, which introduces significant image distortion and limits the bandwidth of the vertical feedback controller. Using Finite Element Analysis (FEA), the first bending-mode resonance frequency of an SCMAP07 actuator in the fixed-free configuration was determined to be 43 kHz. The first piston-mode resonance frequency was much higher at 103 kHz. To increase the lowest mechanical resonance frequency, two options are considered: (1) reduce the overall length of the actuator; and (2) use a compliant flexure to increase the stiffness of the actuator in the transverse directions (x and y).

To increase the resonance frequency, one option is to reduce the actuator length, however, this also reduces the travel range. The 4-mm long actuator considered above consists of a 2-mm thick plate-stack actuator sandwiched between two 1-mm thick ceramic end caps. As recommended by the manufacturer, the end caps provide electrical isolation when the actuator is attached to a conducting substrate. To reduce the actuator length, the 1-mm ceramic end caps were replaced by 0.6 mm thick alumina plate

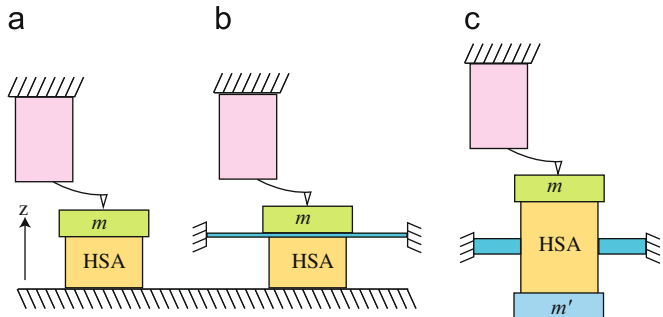


Fig. 5. Mounting configurations for a high-speed piezoelectric stack actuator (HSA) with sample mass m : (a) fixed-free configuration, (b) fixed-free with flexure guidance, and (c) inertial cancellation with a dummy mass m' . The actuation direction is denoted by z .

($E=300$ GPa). As a result, the actuator length was reduced by 20% to 3.2 mm. The modulus of the end caps was also increased by nearly 10 times. The FEA results for this case show that the first bending and piston modes were increased to 72 and 160 kHz, respectively. By reducing the overall actuator length and increasing the effective stiffness, the resonance frequencies were significantly increased.

To further increase the resonance frequency of the bending mode, a circular plate flexure is proposed to increase the stiffness in the transverse directions (x and y) and to guide the sample mass in the z direction [see Fig. 5(b)]. A flexure was also used in Fantner et al. [15] to increase the lateral stiffness of the vertical actuator. The flexure stiffness k_f in the z direction should be less than 10% of the actuator stiffness to minimize the loss of travel range. The flexure material is stainless steel ($E=200$ GPa), with a thickness of 0.254 mm (0.010 in).

The flexure diameter is determined from its required stiffness, which should be around 10% of the actuator stiffness as discussed above. The stiffness of a circular flexure can be derived from the expression for vertical deformation given in [50],

$$\delta_z = \frac{wa^3}{C_1} \left(\frac{C_2 C_3}{C_4} - C_5 \right), \quad (6)$$

where the constants C_i , for $i=1,2,\dots,5$, are

$$C_1 = \frac{Et^3}{12(1-v^2)}, \quad (7)$$

$$C_2 = \frac{1}{4} \left[1 - \left(\frac{b}{a} \right)^2 \left(1 + 2 \ln \left(\frac{a}{b} \right) \right) \right], \quad (8)$$

$$C_3 = \frac{r_0}{4a} \left[\left(\frac{r_0}{a} \right)^2 1 + 2 \ln \left(\frac{a}{r_0} \right) \right], \quad (9)$$

$$C_4 = \frac{1}{2} \left[1 - \left(\frac{b}{a} \right)^2 \right], \quad (10)$$

$$C_5 = \frac{r_0}{4a} \left\{ \left[\left(\frac{r_0}{a} \right)^2 + 1 \right] \ln \left(\frac{a}{r_0} \right) + \left(\frac{r_0}{a} \right)^2 - 1 \right\}. \quad (11)$$

In the above constants, v is Poisson's ratio, a is the radius of the inside constraint, b is the radius of the outside constraint, r_0 is the radius at which the load is applied, and w is the radially distributed load at a radius of r_0 ($w=F/2\pi r_0$) (outer edge of the center guide). Therefore, the stiffness of the circular flexure along the actuation direction z is

$$k_f = \frac{F}{\delta_z} = \frac{2\pi r_0 C_1}{a^3} \left(\frac{C_2 C_3}{C_4} - C_5 \right)^{-1}. \quad (12)$$

In addition to improving the resonance frequencies, it is also necessary to consider the inertial forces generated by accelerating the sample mass at high speed [21]. Inertial forces can excite mechanical resonances of the stage body and also the entire microscope. To cancel inertial forces, the balanced scheme proposed by Ando and co-workers [14,21,31] is adopted. This configuration is illustrated in Figs. 5(c) and 6. For optimum performance, the dummy mass m' is equal to the mass of the sample. The two piezoactuators are electrically connected in parallel, thus both actuators expand and contract simultaneously but in opposite directions. The net effect is cancellation of inertial forces.

In the mechanical assembly, Fig. 6(a), the stage body is machined from a cylindrical piece of stainless steel. Two opposing pockets are machined into the steel slug to accommodate two, 2-mm thick piezo-stack actuators with alumina end caps (each 0.65 mm thick) for electrical isolation. In the final design, plate-stack actuators (5 × 5 mm Nolac CMAP07) were chosen

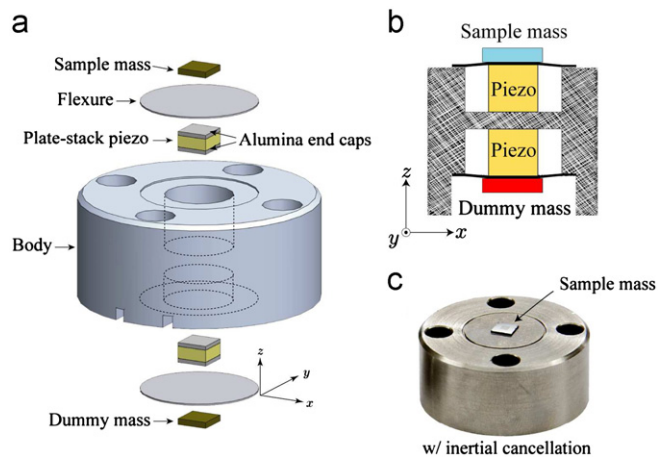


Fig. 6. The vertical positioning stage with inertial cancellation. Assembly drawing (a), mechanical diagram (b), and photograph (c).

over ring-stack actuators due to their lower cost. The main advantage of a ring-stack actuator is the constant annular stress distribution when used with a circular plate flexure. The stress distribution when using a plate-stack actuator is concentrated at the corners of the actuator, which is less desirable.

During assembly, the alumina end caps were first bonded to the actuator using epoxy adhesive. The actuators and circular plate flexures were then bonded under pressure to the stage body. A photograph of the completed assembly with an attached sample mass is shown in Fig. 6(c). The measured full range at 200 V was 2.3 μm.

In addition to the mechanical performance of the positioner, the electrical limitations imposed by the driving amplifier are also important [51]. To maximize the electrical bandwidth, a voltage amplifier with a low AC output impedance was used to drive the actuator (PiezoDrive PDX200). This provided a loaded bandwidth of greater than 100 kHz which does not significantly reduce the maximum bandwidth imposed by the mechanical resonance.

Due to the required control-loop bandwidth, a digital implementation of the controller is not practical. To guarantee a phase-lag of less than 12 degrees at the resonance frequency, the sampling rate would need to be greater than 3 MHz. An analog integral controller is a better alternative that does not suffer from finite resolution or sampling delay.

A simplified schematic diagram of the vertical feedback controller is shown in Fig. 7. The first stage of the circuit is a summer with an optional input v_1 for measuring the closed-loop response of the system. The following integration stage has a gain of $1/R_3 C_3$. The final stage corrects for the integrator inversion and adds an additional signal v_2 . This signal can be used to simulate a sample topography and measure the open-loop response of the vertical positioning system. When measuring the open-loop response, the probe should be kept in contact with the sample by using an extremely low feedback gain. Since the voltage applied to the piezo is proportional to the inverted topography, the topography is best recorded from the output of the integrator as shown.

With the high-speed positioner in place, the open-loop frequency response of the vertical feedback system is plotted in Fig. 3(d). The lowest resonance frequency now occurs at 103 kHz, which is 150 times faster than the piezoelectric tube. In addition to the higher resonance frequency, the peak magnitude is also lower which allows a controller gain of 190×10^3 with a gain-margin of 5 dB. This provides a closed-loop bandwidth of 67 kHz which is an improvement of over 800 times and easily sufficient for line-rates of 200 Hz.

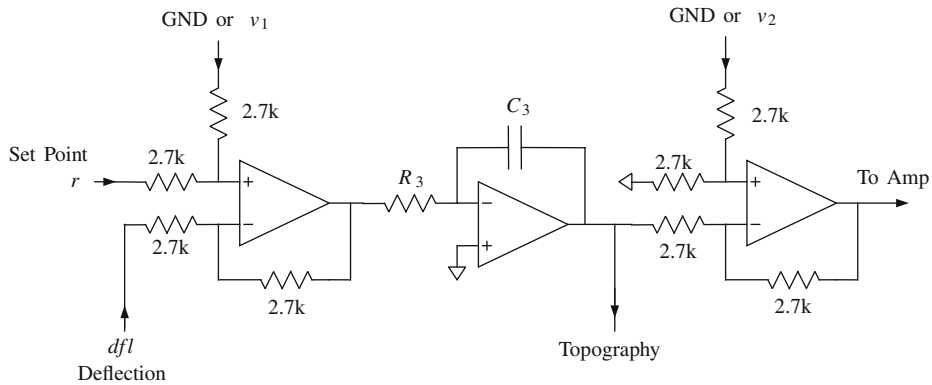


Fig. 7. Simplified schematic diagram of the vertical feedback controller. An LT1362 quad high-speed opamp IC is recommended.

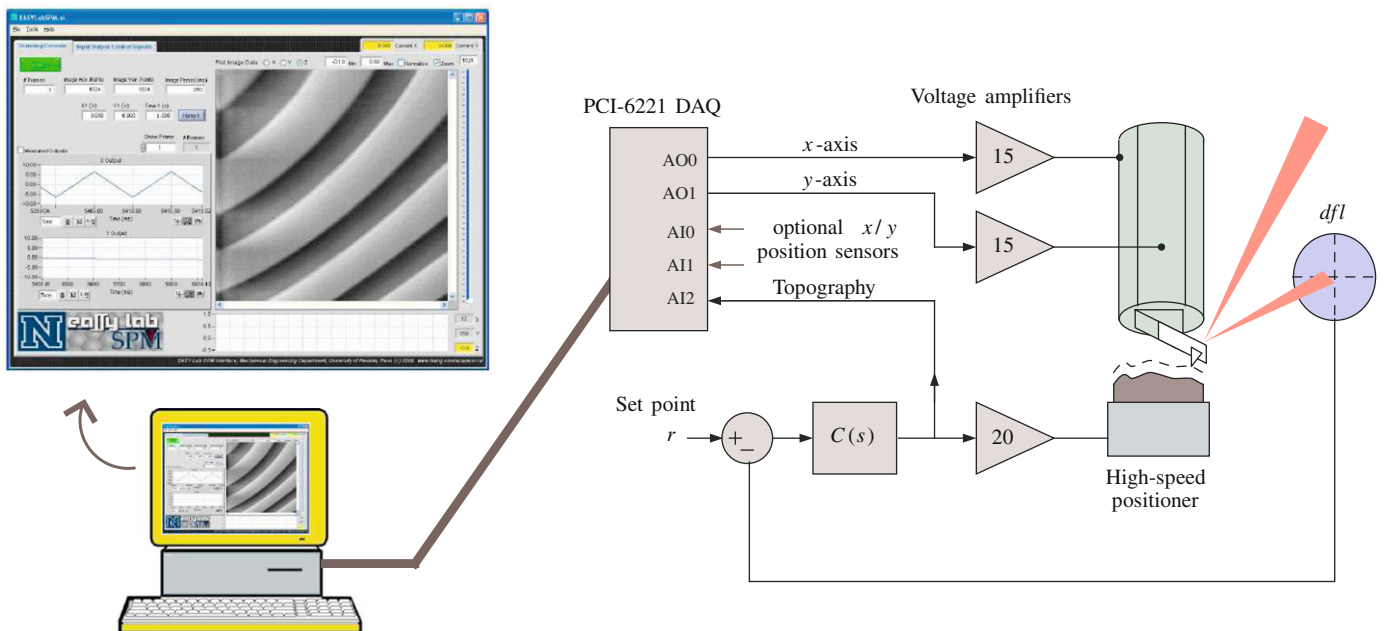


Fig. 8. The microscope control system operating in constant-force contact-mode. The scan generation and image acquisition is performed by the easyLab SPM software and data acquisition card.¹ The analog feedback controller in Fig. 7 regulates the force and produces the topography signal.

The improvement in imaging response when using the high-speed vertical positioner is illustrated in Fig. 4. While the standard feedback system is limited to around 1 Hz, the high-speed controller clearly provides excellent feature tracking, even at line-rates of 200 Hz.

5. Data acquisition

To implement alternative vertical positioning and scanning techniques, the microscope control logic must be modified. If the vendor's software does not provide sufficient flexibility or sampling rate, it must be bypassed. The required functions include generation of the scanning trajectories and acquisition of the cantilever deflection or control signal.

A new microscope controller 'easyLab SPM' has been developed at the University of Nevada, Reno and is available free for educational or research use.¹ This LabView-based program includes scan generation, image acquisition, and a graphical user interface (GUI). A screen shot and the connection diagram is

shown in Fig. 8. The software is compatible with National Instruments data acquisition cards that support the NI-DAQmx drivers. One such card is the NI PCI-6115 high-speed simultaneous sampling data acquisition card, with an analog-to-digital conversion bandwidth of 10 MS/s and a digital-to-analog conversion bandwidth of 2.5 MS/s. This is sufficient for a line rate of 8 kHz and operation at 50 frames-per-second with a resolution of 160×160 . As the scan-rate of the microscope used in this work is limited to approximately 200 Hz, a lower-cost National Instruments PCI-6221 data acquisition card is sufficient. This board contains a 16-channel 16-bit 250 kS/s analog-to-digital converter and two 16-bit analog outputs.

It is important to note that although the data acquisition card has a high sampling-rate, the real-time through-put of LabView is limited to approximately 1 kHz. However, this is not problematic as the only real-time feedback controller is implemented by an analog circuit. This arrangement significantly reduces the system cost and complexity as a DSP system is not required. The easyLab SPM software can also record the actual x- and y-axis displacement if position sensors are available. The acquired image is then plotted against the measured x- and y-axis data rather than the generated scan patterns. This method

¹ The easyLab SPM Interface is available by contacting K.K. Leang.

is appropriate for high-speed AFM where closed-loop lateral positioning may not be practical.

6. Imaging experiments

In this section the imaging performance of the proposed techniques are evaluated and compared to a standard microscope controller. The four control schemes are standard and high-speed vertical feedback with triangular or sinusoidal lateral scan trajectories. The sample under consideration is a Budget Sensors HS-100 MG calibration grating with 116 nm cylindrical features.

In Fig. 9(a) a standard microscope controller and triangular trajectory is used. With a 1 Hz scan-rate the image is ideal with sharp edges and no detectable lateral vibration. However, at 10 Hz scan-rate and above the vertical feedback bandwidth of 83 Hz is not sufficient to track the sample features. In Fig. 9(b), the use of a sinusoidal trajectory offers no improvement as the major limitation is vertical feedback performance.

With high-speed vertical positioning in Fig. 9(c) the vertical response is no longer a limitation. Instead, lateral vibration produces unacceptable image distortion at scan-rates of 10 Hz and above. In Fig. 9(d) the use of a sinusoidal trajectory eliminates the lateral vibration and produces only slight distortion at 200 Hz. The image has sharp edges and is comparable in quality to

that recorded at 1 Hz with the standard microscope controller. This reduces the acquisition time from over three minutes to one second for a 200×200 resolution image, an improvement of 200 times.

7. Conclusions

The imaging speed of a scanning probe microscope is typically limited to less than one image per minute. This is due to the low performance of the vertical feedback loop, the lateral positioner and the data acquisition system. In this work, these limitations are overcome by the combination of high-speed vertical positioning, sinusoidal lateral scanning and high-speed data acquisition.

By using a sinusoidal rather than triangular scanning trajectory, the maximum scan-rate of a piezoelectric tube was increased from around 1 to 200 Hz. At these speeds, a standard vertical feedback controller cannot adequately track sharp sample features. To improve the vertical feedback bandwidth, the standard piezoelectric tube positioner was replaced by a high-speed stack based positioner. This simple modification increased the closed-loop bandwidth from 83 Hz to 67 kHz, an improvement of over 800 times. The faster vertical feedback was demonstrated to provide excellent feature tracking even at scan-rates of 200 Hz.

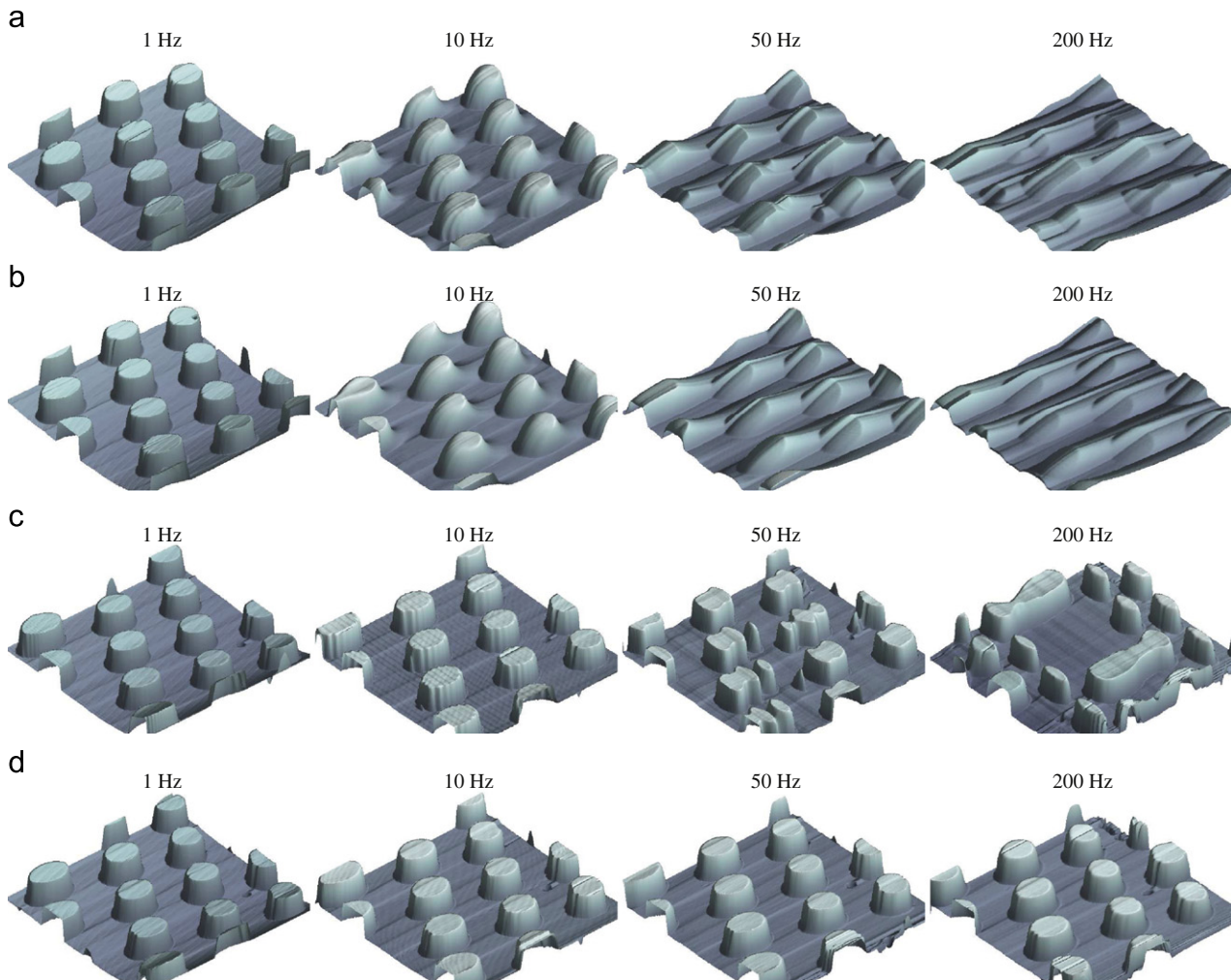


Fig. 9. A comparison of imaging performance with different scanning and vertical feedback techniques. The sample is a Budget Sensors HS-100 MG calibration grating imaged in constant-force contact-mode scan with a range of $20 \times 20 \mu\text{m}$. The feature height is 116 nm. (a) Standard vertical feedback with triangular scanning, (b) standard vertical feedback with sinusoidal scanning, (c) high-speed vertical feedback with triangular scanning, and (d) high-speed vertical feedback with sinusoidal scanning.

To permit the ready application of this work to any microscope, a LabView based image acquisition system was developed. This system replaces the scan generation and recording functions of a standard microscope controller.

In experiments, the above techniques were demonstrated to increase the scan-rate of an NT-MDT Ntegra microscope from 1 to 200 Hz without sacrificing image quality. This reduces the image acquisition time from more than 3 min to 1 s. At this speed, a standard microscope can be used to observe dynamic processes and to drastically increase the throughput of nanofabrication and inspection tasks.

Future work includes the extension to other imaging modes such as SNOM. There is also scope to reduce the image acquisition time to 100 ms while retaining standard microscope hardware.

Acknowledgments

This research was supported by the Australian Research Council (DP0666620), the Center for Complex Dynamic Systems and Control, and in part by the Nevada NASA Space Grant Consortium. Experiments were conducted at the Laboratory for Dynamics and Control of Nanosystems, University of Newcastle. Authors also thank Tony Berendsen, Development Technician in the Mechanical Engineering Department at the University of Nevada, Reno, for his help fabricating the flexure-guided z-axis stage.

References

- [1] M.J. Brukman, D.A. Bonnell, Probing physical properties at the nanoscale, *Physics Today* 61 (6) (2008) 36–42.
- [2] Y.F. Dufrêne, Towards nanomicrobiology using atomic force microscopy, *Nature Reviews Microbiology* 6 (2008) 674–680.
- [3] N. Jalili, K. Laxminarayana, A review of atomic force microscopy imaging systems: application to molecular metrology and biological sciences, *Mechatronics* 14 (8) (2004) 907–945.
- [4] E. Meyer, H.J. Hug, R. Bennewitz, Scanning probe microscopy, *The Lab on a Tip*, Springer-Verlag, Heidelberg, Germany, 2004.
- [5] B. Bhushan, H. Fuchs (Eds.), *Applied Scanning Probe Methods (I–X)*, Springer-Verlag, Heidelberg, Germany, 2006.
- [6] G. Binnig, C.F. Quate, C. Gerber, Atomic force microscope, *Physical Review Letters* 56 (9) (1986) 930–933.
- [7] G. Borionetti, A. Bazzalà, R. Orizio, Atomic force microscopy: a powerful tool for surface defect and morphology inspection in semiconductor industry, *The European Physical Journal Applied Physics* 27 (1–3) (2004) 101–106.
- [8] A. Humphris, M. McConnell, D. Catto, A high-speed atomic force microscope capable of video-rate imaging, *Microscopy and Analysis—SPM Supplement* 7 (2006) 29–31.
- [9] A. Ferreira, C. Mavroidis, Virtual reality and haptics for nanorobotics, *IEEE Robotics and Automation Magazine* 13 (3) (2006) 78–92.
- [10] A.A. Tseng, S. Jou, A. Notargiacomo, T.P. Chen, Recent developments in tip-based nanofabrication and its roadmap, *Journal of Nanoscience and Nanotechnology* 8 (5) (2008) 2167–2186.
- [11] A.A. Tseng (Ed.), *Nanofabrication: Fundamentals and Applications*, World Scientific, Singapore, 2008.
- [12] J.A. Vicary, M.J. Miles, Pushing the boundaries of local oxidation nanolithography: short timescales and high speeds, *Ultramicroscopy* 108 (10) (2008) 1120–1123.
- [13] G. Schitter, R.W. Stark, A. Stemmer, Fast contact-mode atomic force microscopy on biological specimens by model-based control, *Ultramicroscopy* 100 (2004) 253–257.
- [14] T. Ando, N. Kodera, T. Uchihashi, A. Miyagi, R. Nakakita, H. Yamashita, K. Matada, High-speed atomic force microscopy for capturing dynamic behavior of protein molecules at work, *e-Journal of Surface Science and Nanotechnology* 3 (2005) 384–392.
- [15] G.E. Fantner, G. Schitter, J.H. Kindt, T. Ivanov, K. Ivanova, R. Patel, N. Holten-Andersen, J. Adams, P.J. Thurner, I.W. Rangelow, P.K. Hansma, Components for high speed atomic force microscopy, *Ultramicroscopy* 106 (2–3) (2006) 881–887.
- [16] M. Kobayashi, K. Sumimoto, K. Torimitsu, Real-time imaging of DNA-streptavidin complex formation in solution using a high-speed atomic force microscope, *Ultramicroscopy* 107 (2–3) (2007) 184–190.
- [17] A.J. Fleming, Dual-stage vertical feedback for high speed-scanning probe microscopy, *IEEE Transactions on Control Systems Technology*, in press, doi:10.1109/TCST.2010.2040282.
- [18] D.Y. Abramovitch, S.B. Andersson, L.Y. Pao, G. Schitter, A tutorial on the mechanisms, dynamics, and control of atomic force microscopes, in: Proceedings of the American Control Conference, New York City, NY, 2007, pp. 3488–3502.
- [19] S.M. Salapaka, M.V. Salapaka, Scanning probe microscopy, *IEEE Control Systems Magazine* 28 (2) (2008) 65–83.
- [20] G. Schitter, Improving the speed of AFM by mechatronic design and modern control methods, *Technisches Messen* 76 (5) (2009) 266–273.
- [21] T. Ando, T. Uchihashi, T. Fukuma, High-speed atomic force microscopy for nano-visualization of dynamic biomolecular processes, *Progress in Surface Science* 83 (7–9) (2008) 337–437.
- [22] A.J. Fleming, S.O.R. Moheimani, Sensorless vibration suppression and scan compensation for piezoelectric tube nanopositioners, *IEEE Transactions on Control Systems Technology* 14 (1) (2006) 33–44.
- [23] S. Devasia, E. Eleftheriou, S.O.R. Moheimani, A survey of control issues in nanopositioning, *IEEE Transactions on Control Systems Technology* 15 (5) (2007) 802–823.
- [24] A.J. Fleming, K.K. Leang, Charge drives for scanning probe microscope positioning stages, *Ultramicroscopy* 108 (12) (2008) 1551–1557.
- [25] G.M. Clayton, S. Tien, K.K. Leang, Q. Zou, S. Devasia, A review of feedforward control approaches in nanopositioning for high-speed SPM, *Journal of Dynamic Systems, Measurement, and Control* 131 (2009) 061101(1–19).
- [26] J. Vaughan, W.S.A. Yano, Robust negative input shapers for vibration suppression, *Journal of Dynamic Systems, Measurement, and Control* 131 (2009) 031014(1–9).
- [27] A.J. Fleming, A.G. Wills, Optimal periodic trajectories for band-limited systems, *IEEE Transactions on Control Systems Technology* 13 (3) (2005) 552–562.
- [28] G. Schitter, K.J. Åström, B.E. DeMartini, P.J. Thurner, K.L. Turner, P.K. Hansma, Design and modeling of a high-speed AFM-scanner, *IEEE Transactions on Control Systems Technology* 15 (5) (2007) 906–915.
- [29] T. Ando, Control techniques in high-speed atomic force microscopy, in: Proceedings of the American Control Conference, Seattle, WA, 2008, pp. 3194–3200.
- [30] S.O.R. Moheimani, Accurate and fast nanopositioning with piezoelectric tube scanners: emerging trends and future challenges, *Review of Scientific Instruments* 79 (7) (2008) 071101(1–11).
- [31] T. Ando, N. Koder, E. Takai, D. Maruyama, K. Saito, A. Toda, A high-speed atomic force microscope for studying biological macromolecules, *Proceedings of the National Academy of Sciences* 98 (22) (2001) 12468–12472.
- [32] A.D. Humphris, M.J. Miles, J.K. Hobbs, A mechanical microscope: high-speed atomic force microscopy, *Applied Physics Letters* 86 (2005) 034106(1–3).
- [33] M.J. Rost, L. Crama, P. Schakel, E. van Tol, G.B.E.M. van Velzen-Williams, C.F. Overgaauw, H. ter Horst, H. Dekker, B. Okhuijsen, M. Seynen, A. Vijftigchild, P. Han, A.J. Katan, K. Schoots, R. Schumm, W. van Loo, T.H. Oosterkamp, J.W.M. Frenken, Scanning probe microscopes go video rate and beyond, *Review of Scientific Instruments* 76 (5) (2005) 053710(1–9).
- [34] L.M. Picco, L. Bozec, A. Ulcinas, D.J. Engledew, M. Antognazzi, M. Horton, M.J. Miles, Breaking the speed limit with atomic force microscopy, *Nanotechnology* 18 (4) (2007) 044030(1–4).
- [35] K.K. Leang, Iterative learning control of hysteresis in piezo-based nanopositioners: theory and application in atomic force microscopes, Ph.D. Thesis, University of Washington, 2003.
- [36] S.-K. Hung, Spiral scanning method for atomic force microscopy, in: Proceedings of the Tip Based Nanofabrication Workshop, Taipei, Taiwan, 2008, pp. 10(1–10).
- [37] D.Y. Abramovitch, D.P. Fromm, D. Schroeder, Scanning probe microscope with improved scanning speed, US Patent US2009/0107222, 2009.
- [38] I.A. Mahmood, S.O.R. Moheimani, B.Bhikkaji, A new scanning method for fast atomic force microscopy, *IEEE Transactions on Nanotechnology*, in press, doi:10.1109/TNANO.2009.2036844.
- [39] G. Kwon, S. Kim, M. Jeong, S. Han, C. Choi, S. Han, J. Hong, H. Lee, High-speed atomic force microscope lithography using a piezotube scanner driven by a sinusoidal waveform, *Ultramicroscopy* 109 (8) (2009) 1052–1055.
- [40] M.J. Rost, G.J.C. van Baarle, A.J. Katan, W.M. van Spengen, P. Schakel, W.A. van Loo, Video-rate scanning probe control challenges: setting the stage for a microscopy revolution, *Asian Journal of Control* 11 (2) (2009) 110–129.
- [41] T. Sulcik, S.C. Minne, J.D. Adams, D.A. Fletcher, A. Atalar, C.F. Quate, D.M. Adderton, Dual integrated actuators for extended range high speed atomic force microscopy, *Applied Physics Letters* 75 (11) (1999) 1637–1639.
- [42] Y. Jeong, G.R. Jayanth, C.-H. Menq, Control of tip-to-sample distance in atomic force microscopy: a dual-actuator tip-motion control scheme, *Review of Scientific Instruments* 78 (9) (2007) 093706(1–7).
- [43] T. Akiyama, U. Stauffer, N.F. de Rooij, Atomic force microscopy using an integrated comb-shape electrostatic actuator for high-speed feedback motion, *Applied Physics Letters* 76 (21) (2000) 3139–3141.
- [44] Y. Yan, Y. Wu, Q. Zou, C. Su, An integrated approach to piezoactuator positioning in high-speed atomic force microscope imaging, *Review of Scientific Instruments* 79 (2008) 073704(1–9).
- [45] G. Schitter, W.F. Rijkée, N. Phan, Dual actuation for high-bandwidth nanopositioning, in: Proceedings of the IEEE Conference on Decision and Control, Cancun, Mexico, 2008, pp. 5176–5181.
- [46] C. Prater, C. Su, N. Phan, J.M. Markakis, C. Cusworth, J. Shi, J.H. Kindt, S.F. Nagle, W. Fan, Fast scanning SPM and method of operating same, US Patent US2009/0032706, 2009.
- [47] A.J. Fleming, S.S. Aphale, S.O.R. Moheimani, A new method for robust damping and tracking control of scanning probe microscope positioning

- stages, IEEE Transactions on Nanotechnology, in press, doi:10.1109/TNA-NO.2009.2032418.
- [48] G. Schitter, P.J. Thurner, P.K. Hansma, Design and input-shaping control of a novel scanner for high-speed atomic force microscopy, Mechatronics 18 (5–6) (2008) 282–288.
- [49] J. Maess, A.J. Fleming, F. Allgöwer, Simulation of dynamics-coupling in piezoelectric tube scanners by reduced order finite element models, Review of Scientific Instruments 79 (2008) 015105(1–9).
- [50] W.C. Young, R.G. Budynas, Roark's Formula for Stress and Strain, seventh ed., McGraw-Hill, New York, 2002.
- [51] A.J. Fleming, A MHz bandwidth dual-amplifier for driving piezoelectric actuators and other highly capacitive loads, Review of Scientific Instruments 80 (2009) 104701(1–7).